Catalysis Communications 173 (2023) 106560

Contents lists available at ScienceDirect

Catalysis Communications

journal homepage: www.elsevier.com/locate/catcom

Green and facile synthesis of strontium doped Nb_2O_5/RGO photocatalyst: Efficacy towards H_2 evolution, benzophenone-3 degradation and Cr (VI) reduction

K. Yogesh Kumar [a], M.K. Prashanth [b], H. Shanavaz [a], L. Parashuram [c], Fahad A. Alharti [d], Byong-Hun Jeon [e,*], M.S. Raghu [f,*]

[a] Department of Chemistry, Faculty of Engineering and Technology, Jain University, Bangalore 562112, India
[b] Department of Chemistry, BNM Institute of Technology, Banashankari, Bangalore 560070, India
[c] Department of Chemistry, Nitte Meenakshi Institute of Technology, Yelahanka, Bangalore 560064, India
[d] Department of Chemistry, College of Science, King Saud University, Riyadh 11451, Saudi Arabia
[e] Department of Earth Resources and Environmental Engineering, Hanyang University, 222, Wangsimni-ro, Seongdong-gu, Seoul 04763, Republic of Korea
[f] Department of Chemistry, New Horizon College of Engineering, Outer Ring Road, Bangalore 560103, India

ARTICLE INFO

Keywords:
Sr doped Nb_2O_5/RGO
Effect of doping
Photocatalysis
H_2 evolution
Benzophenone-3
Cr(VI)

ABSTRACT

A simple co-precipitation method has been developed to synthesize Nb_2O_5/reduced graphene oxide nanocomposite (NbO/RGO). The effect of various % of strontium doping on NbO/RGO was studied. The characterization results for its structure; morphology confirms the decoration of NbO with RGO followed by Sr doping resulting in Sr@N/R-wt% nanocomposite. Various % of Sr has been doped to NbO/RGO and evaluated for photocatalytic H_2 evolution, degradation benzophenone-3, and Cr(VI). Enhanced H_2 evolution was observed in Sr@N/R-0.75% nanocomposite (1925 μmol) and found three and two times greater than pristine NbO and NbO/RGO, respectively. Sr@N/R-0.75% nanocomposite was able to degrade 94.6 and 87.7% of BP and Cr(VI) respectively.

1. Introduction

Industrialization and urbanization across the globe have led to a huge demand for energy which is causing energy scarcity and environmental pollution indirectly. The energy sources like fossil fuels need alternate sources of energy that can meet the energy demand and reduce environmental contamination [1]. Hydrogen is a fuel that burns with zero emission with high energy density. Classical hydrogen evolution utilizes Pt, Ru, and Pd as electrocatalysts which are costly and consume lot of energy in the form of electricity [2]. Recently, photocatalytic hydrogen evolution technology has gained high prominence due to its eco-friendly nature, no electricity consumption etc. [3].

Along with the energy sector, environmental pollution particularly water treatment needs lot of improvement. Water contamination due to the accumulation of heavy metals, Cr(VI), personal care products, synthetic dyes, pesticides, and insecticides causes ecological imbalance and is a threat to living beings [4]. People use many organic compounds in their day to day life like, cosmetics, shampoo, hair spray, deodorant, perfumes, detergents, makeup, etc. These are covered under a separate class of pollutants of emerging concern since their impact is not explored and they are not regulated [5].UV filters like Benzophenone-3 (2-hydroxy-4-methoxyphenyl) phenylmethanone) are extensively used in sunscreen lotions, cosmetics etc. by human beings to avoid exposure to UV radiations. BP is an organic UV filter that can only absorb specific wavelength range of radiation and hence offer protection to the skin. BP and other personal care products are made to discharge into the water bodies and soil without any concern [6]. This leads to environmental pollution which persists for a longer time due to the complex structures and causes ecological imbalance. BP has been identified in surface water, swimming pools as well as in fish. BP of 10% concentration in sunscreen could penetrate the human body in several hours and disrupts the endocrine, nervous system, hormonal system etc. [7]. Chromium is an inorganic compound that has been used extensively in leather industries, electroplating, mining, etc. The toxicity of Cr is high in its Cr (VI) state compared to Cr(III) state. The upper limit for Cr(VI) in water is 0.05 mg L^{-1} beyond this leads to cancer, liver damage etc. [8]. By

* Corresponding authors.
E-mail addresses: bhjeon@hanyang.ac.kr (B.-H. Jeon), dr.msraghu@newhorizonindia.edu (M.S. Raghu).

https://doi.org/10.1016/j.catcom.2022.106560
Received 15 September 2022; Received in revised form 28 October 2022; Accepted 6 November 2022
Available online 8 November 2022

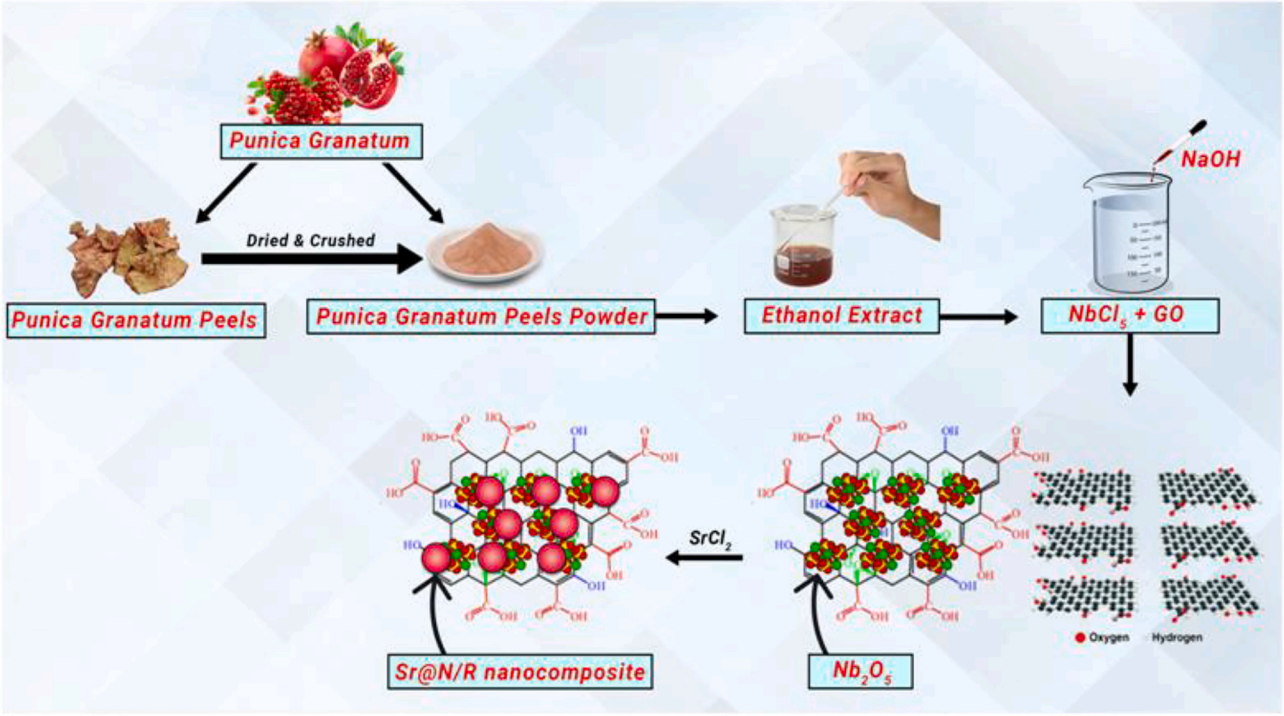

Scheme 1. Synthesis of NbO/RGO and Sr@N/R nanocomposite.

looking into the need for green energy and adverse effects of pollutants in the water among the life of living beings, the production of H_2 and pollutant treatment is in high demand.

The multifunctional materials that can tackle both energy and environmental related issues are of great concern among researchers. Compare to many other methods available for the removal of pollutants from water, photocatalytic treatment has maximum advantages, since it completely converts the pollutants to less toxic/harmless products [9]. The main characteristics of materials to exhibit photocatalytic properties involve high surface area, low bandgap, good conductivity, electron-hole separation, ability to generate active species in presence of dissolved oxygen, ability to absorb visible light, etc. [10]. Several metal oxides like TiO_2, RuO_2, ZrO_2, V_2O_5, Ta_2O_5, ZnO, and CuO have been extensively used for hydrogen evolution and photocatalytic degradation [11]. Nb_2O_5 (NbO) is one of the promising metal oxides with lowered bandgap (~3.2 eV), and good conductivity that is used in several studies like hydrogen evolution, batteries, adsorption, supercapacitors and solar cells [12]. The limitation of NbO is its lower stability towards advanced oxidation process due to fast recombination of photo-excited electrons and holes, incomplete absorption of visible light, low conductivity, etc. [13].

Hence NbO is to be decorated with other metal oxides, graphene-based compounds or other two-dimensional materials. Reduced graphene oxide has been used by several researchers as a matrix material to enhance the photocatalytic efficiency of host materials. RGO exhibits high surface area, superior conductivity, flexibility, high young's modulus, and easy functionalization with other metal oxides [14]. To further enhance the light-driven activity of NbO/RGO nanocomposite it is doped with abundantly available alkaline earth metal strontium. Doping of Sr to NbO/RGO could help in reducing the bandgap by generating energy states in the forbidden gap and also creating an electron trapping site for photoexcited electrons/holes [15]. In addition, there could be a structural modification, defects due to variation in the ionic radius, increase in surface area, conductivity, and morphological changes that show its effect on the advanced oxidation process [16].

The methods available for the synthesis of metal oxide/Graphene based nanocomposite include solvo/hydrothermal method, microemulsion approach and sol-gel etc. [17]. Developments of methods which are simple to the above-said methods are on demand. Reduction of GO has been done by many methods like photo-reduction, microwave reduction, electrochemical reduction as well as chemical reduction. The results of the chemical reduction method were most explored due to economic and effective degree of reduction. The reducing agents used in chemical reduction usually involve sodium borohydride, strong alkalies, hydrazine hydrate, hydrohalic acid and dimethylhydrazine [18]. Though, these reducing agents show good properties exhibiting toxicity to the health and environment. Hence environmental benign approach using biomass, agro wastes etc. could help in partial reduction of environmental pollution and a great decrease in the reduction of toxicity, cost etc. [19]. Green synthesis of metal oxide/RGO nanocomposites was greatly explored by several scientists that involve wealth from waste, low energy, replacing toxic solvents etc. *Punica Granatum* (Pomegranate) is a fruit consumed worldwide and sometimes uses its peels and leaves of them as agro wastes [20]. The peel of pomegranate consists of several organic compounds like polyphenols, punicalin, punicalagin and ellagitannins and is used as antioxidants. These phytoconstituents have been used as reducing agents in many metal oxide nanoparticle synthesis [21].

Punica Granatum peel extract has been used as a reducing agent for the synthesis of Sr doped Nb_2O_5/RGO nanocomposite. The method involves a simple precipitation approach which gives the Sr@N/R nanocomposite. The developed method does not involve any high energy radiations or temperature and the reaction is processed at room temperature. A slight agglomeration is observed in the nanocomposite, which is confirmed by the morphological characterization. The effect of doping of Sr % to NbO/RGO nanocomposite has been studied. Sr@N/R-0.75% nanocomposite also subjected to TOC removal in swimming pool water sample. The results reveal that Sr@N/R-0.75% nanocomposite could be a material that probably finds a way for further research in the area of heterogeneous catalysis.

2. Experimental

2.1. Materials

Niobium chloride ($NbCl_5$), Strontium chloride hexahydrate ($SrCl_2.6H_2O$), NaOH, $KMnO_4$, H_2SO_4 and C_2H_5OH, were procured from Fisher Scientific India Pvt. Ltd. in Mumbai, India. All chemicals (Analytical grade reagents, AR) were used in the experiments, without further purifications.

2.2. Preparation Punica Granatum peel extract

Punica Granatum peels were collected from the nearby juice center in Bangalore. Peels were washed thoroughly with water and sundried for 7 days. Completely dried peels were ground thoroughly and then added with 1:2 mixtures of ethanol and water and heated slowly at room temperature for 2 h. the extract obtained was filtered and the supernatant was stored in an air-tight container for further use.

2.3. Preparation of NbO /RGO and Sr@N/R nanocomposite

Graphene oxide (GO) was synthesized by the Modified Hummers method [22]. NbO/RGO nanocomposite was synthesized by using low energy and an economical method called co-precipitation. Wherein, 100 mL of 1 M sodium hydroxide was taken in a 250 mL beaker and stirred continuously for 10 min at room temperature. 0.5 M Niobium chloride hexahydrate solution was added dropwise into the beaker with continuous stirring till white colour precipitate is obtained. In a later stage, 1 mg mL^{-1} of GO solution and 5 mL of *Punica Granatum* Peel extract was added and stirred continuously for 1 h. Sr@NbO/RGO of various wt% (0.25,0.50, 0.75 and 1.0) was prepared by loading a stoichiometric amount of strontium chloride hexahydrate ($SrCl_2.6H_2O$) into the precipitates obtained in the above step. The entire mixture is stirred continuously for an hour. The precipitate is allowed to settle, filtered and washed continuously with water and ethanol thrice to remove all the impurities. Precipitates were collected and dried in an oven at 50 °C for 2 h. In all the above-mentioned experiments, we have used only room temperature except the drying process. The synthetic procedure is clearly figured out in Scheme 1.

2.4. Hydrogen evolution

In a round bottom flask containing 50 mL of water, 25 mg of synthesized catalysts were added and the reaction mixture was purged with N_2 after adding 25 mL of the sacrificial agent. 400 W Xe light was illuminated over the solution. The evolved gas was collected and measured at a thermal conductivity detector in a gas chromatograph.

2.5. Photocatalytic degradation studies of BP and Cr(VI)

A degradation study of benzophenone-3 was examined under UV, visible and sunlight (carried out during summer in Bangalore, India, having 57,000 fluxes). A standard solution (100 mg L^{-1}) of BP was prepared in deionized water and used accordingly after dilution. Under optimum conditions (Fixed pH, initial concentration and catalyst dosage) the BP solution was taken in a round bottom flask and dispersed. Then, the solution was stirred continuously for 30 min to attain adsorption/desorption equilibrium. At an interval of 10 min after light irradiation, a 3 mL aliquot of BP was collected and measured the absorbance using a UV–visible spectrophotometer. The percentage of degradation of BP was calculated using Eq. (1);

$$\%degradation = \frac{C_{0-C}}{C_0} \times 100 \quad (1)$$

where, C_0 and C are initial and final concentrations of the BP, respectively.

The same procedure was followed to calculate the % reduction of Cr (VI) using potassium dichromate solution under optimum conditions.

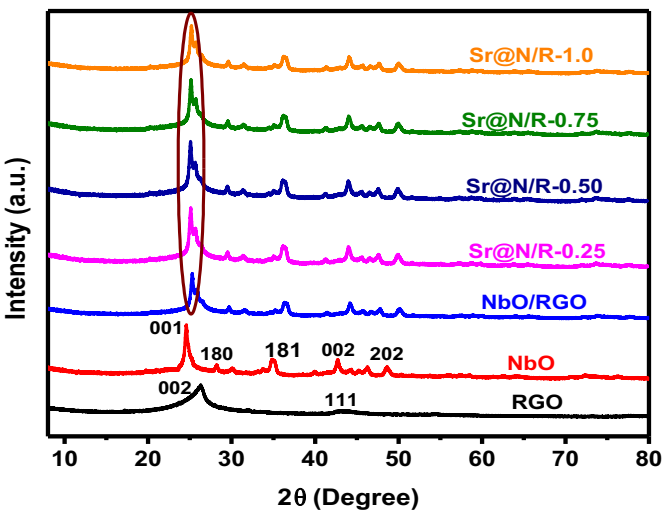

Fig. 1. The X-ray diffraction patterns of RGO, NbO, NbO/RGO, Sr@N/R-0.25%, Sr@N/R-0.5%, Sr@N/R-0.75%, Sr@N/R-1% nanocomposite.

2.6. Characterization

Bruker D2 Phaser XRD equipment was used to analyze the materials' X-ray diffraction (XRD) patterns. The SEM and TEM analyses were conducted using the JEOL JSM 840A and JEOL/JEM 2100, respectively. Omicron spectrometer was used to measure and record X-ray photoelectron spectra. The ASAP 2010 Micrometrics system was used to measure the surface area of the BET. The photoluminescence studies were evaluated using Shimadzu RF-6000 spectroflurometer, while the Shimadzu 1600 model was used to record absorbance.

3. Results and discussion

3.1. Photocatalyst characterization

The crystallanity, degree of purity, nanocomposite formation and crystallographic of the synthesized materials have been examined using X-ray diffraction studies. Fig. 1 shows the XRD patterns of the above-mentioned materials like RGO, NbO, NbO/RGO, and different wt% of Sr@N/R nanocomposites. The peaks in the Fig. 1 indicate the formation of the orthorhombic structure of pure NbO. All the peaks are indexed perfectly to the JCPDS card No. 37–1468 [23]. The peaks obtained at 2 theta and their corresponding diffraction planes are as follows: 24.4°, 28.1°, 35.3°, 42.6° and 48.5° can be ascribed to the (001), (180), (181), (002), and (202). In addition to the peaks of pure NbO a small and broad peak at 2θ ≈ 26° indicates the presence of RGO. The reduction of GO to RGO is confirmed by the XRD of GO (Fig.S1), exhibiting its characteristic peak at 2 theta 10.6 belongs to 001 plane and the absence of broad peak at ≈ 26°. In any of the XRD patterns all the above-said peaks were retained and also there were no extra peaks are observed for SrO and any Sr-based oxides. This indicates that Sr metal is doped on the crystal structure (voids) of NbO. In the later stage when different concentrations of Sr was doped, a slight shift in the peak position and also a decrease in the intensity of the peaks are observed. This shift may be due to the difference in ionic radii of Nb and Sr, and also Sr ions enter into the Nb lattice through interstitial or substitution mode. It is possible that the relatively low concentration of RGO in the composites, which is capped by the high (101) diffraction signal from crystalline NbO, accounts for the absence of a major peak relevant to RGO. Further confirmation of

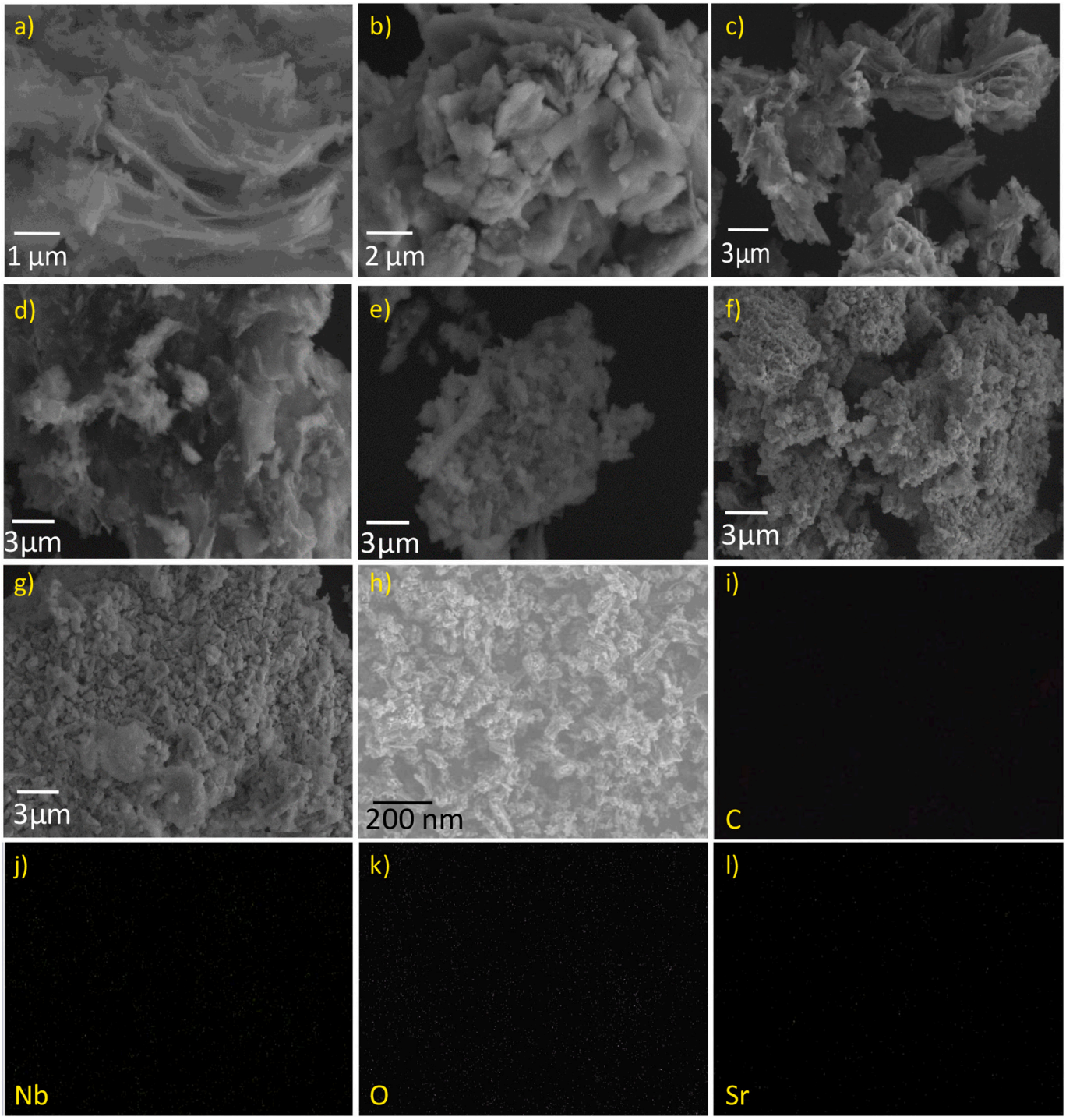

Fig. 2. SEM micrographs of a)RGO, b) NbO c) NbO/RGO d) Sr@N/R-0.25% e)Sr@N/R-0.5% f) Sr@N/R-0.75%, g) Sr@N/R-1% and h-l) EDS mapping of Sr@N/R-0.75% nanocomposite.

reduction of GO to RGO is done through Raman spectroscopic analysis and the obtained spectra is given in Fig.S2.

SEM is one of the powerful tools to study the morphology of the synthesized material. Fig. 2 emphasizes the SEM images of RGO, NbO, NbO/RGO and Sr@N/R nanocomposites at various concentrations. Fig. 2a shows the formation of thin layers of sheet-like structures of RGO which are also stacked over one another. These nanosheets are aligned as a horizontal layer with the crosslinking structures. Fig. 2b illustrates an SEM image of NbO indicates the presence of an irregular pellet-like structure. Fig. 2c shows the image of NbO/RGO nanocomposite which indicates the coexistence of stacked nanosheets and also the distribution of NbO particles on the surface of the sheets. The growth of NbO might have increased the thickness of the sheets and aggregation of the particles are also may be due to the lower temperature used during the reaction. XRD results show the presence of Sr metal in the composite, different concentrations of Sr doped NbO/RGO are shown in the Fig. 2d-g. Images clearly indicates that as the concentration of Sr increased preliminary the sheet-like structure was distorted, crumpled and also layers got separated. With further increase in the concertation of the Sr, nearly globular particles are started to scatter on the top of the

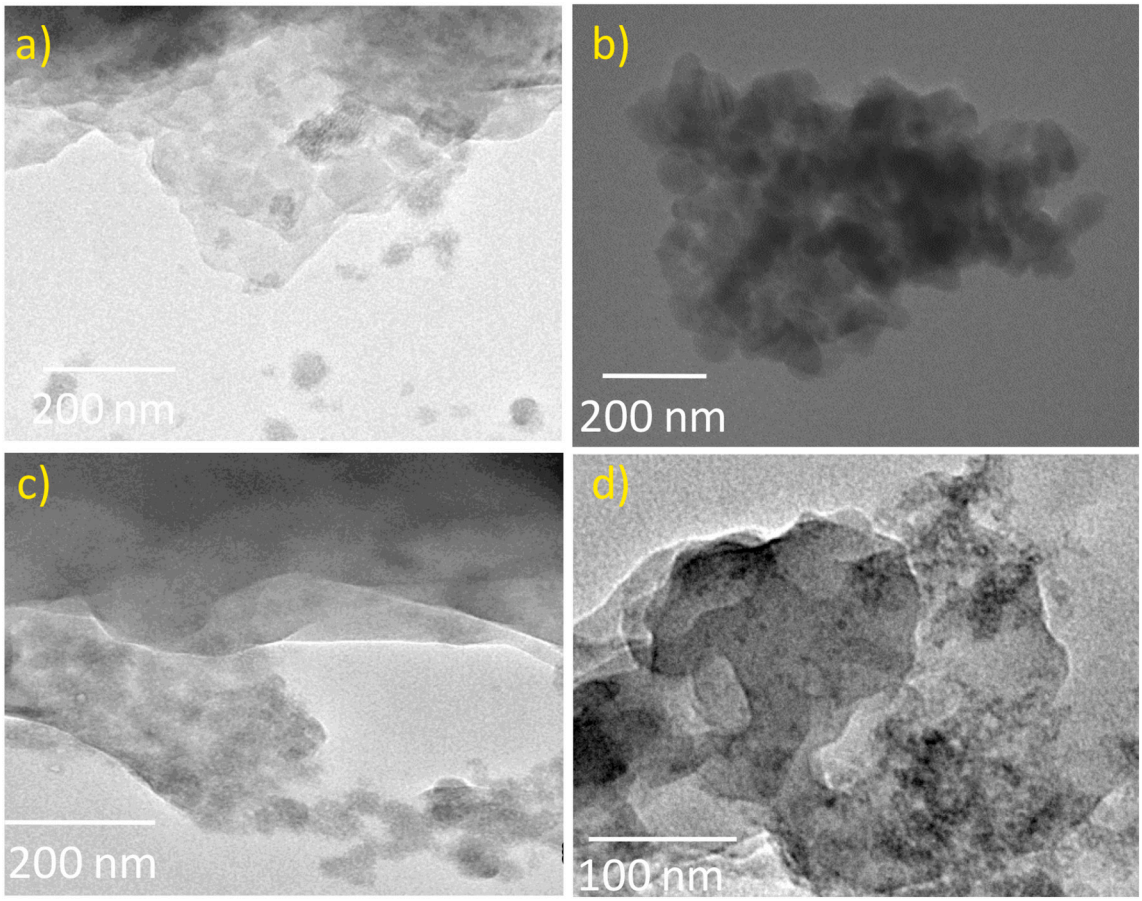

Fig. 3. TEM micrographs of a) RGO, b) NbO c) NbO/RGO and d) Sr@N/R-0.75% nanocomposite.

composites. Whensoever the concentration reaches to 0.50 (Fig. 2e) and 1.0 (Fig. 2g), the Sr particles covered the whole surface of the underneath sheet like NbO/RGO nanocomposites. It indicates that the thickness of the nanosheet layers is increased and only spherical particles are seen from the top view with a lot of aggregation. Fig. 2h-2i shows the elemental mapping results of the Sr@N/R-0.75% nanocomposite, it clearly shows the presence of C, O, Nb, and Sr elements and shows the uniform distribution of all the elements in the Sr@N/R-0.75% nanocomposite.

By using TEM, the morphology and particle size of RGO, NbO, NbO/RGO, and Sr@N/R-0.75% were identified and further investigated. Fig. 3a depicts the sheet like structure of RGO. NbO NPs were displayed in Fig. 3b as a nearly round or flake-shaped structure with a size of 35 nm. The shape of the particles remains unchanged after the NbO to RGO layers are inserted, but there is a clear increase in the size of the particles. Large numbers of NbO particles are unevenly distributed on the layers of RGO, and the structure of the RGO sheets remained the same even after the composites were formed (Fig. 3c). As seen in Fig. 3d, there is a cluster of metal particles that are anchored to the composites' crystal structure after the Sr ions have been added. Additionally, the results are in line with the SEM data, however, in the instance of Sr@N/R-0.75%, we were still able to identify the layers of RGO and distinct particle contrasts.

Fig. 4 shows the XPS analysis of the Sr@N/R-0.75%, survey spectrum (Fig. 4a) shows the signals corresponding to the Sr, Nb, C and O species. XPS of pure NbO and RGO is given in Fig. S3. The presence of Sr ion is confirmed by the peak at binding energies of 133.23 eV and 134.94 eV in the Core Sr 3d spectra displayed in Fig. 4b. Fig. 4c displays the binding energy of the high-resolution Nb 3d spectrum. Niobium pentoxide, Nb $3d_{3/2}$ and Nb $3d_{5/2}$, will correspond to the peaks at 209.92 and 207.25 eV supporting the idea that Nb exists in the +5 oxidation state. Similarly, the peaks located at 532.31 and 530.41 eV in Fig. 4d clearly show the existence of bond between C═O bond, C–OH or C–O–C bond, and Nb—O bond. The peaks observed at 284.13 and 286.82 eV (Fig. 4e) is due to the bond between the carbon and oxygen atom precisely (O–C═O, C═O, C—O bonds). In Sr@N/R-0.75% nanocomposite the Sr substitution significantly increased the release of ions to the target during the photocatalytic dye degradation process.

Further UV-DRS studies of the materials have been examined to evaluate the light-harvesting ability. Fig. 5a shows the absorption spectra of NbO, NbO/RGO and Sr@N/R-0.75% nanocomposite. The light absorption capability of NbO is only up to 380–400 nm, but NbO/RGO and Sr@N/R-0.75% show a blue shift where light absorption ability is found to increase up to around 500 nm. A corresponding plot of photon energy against the Kubelka-Munk factor is given in Fig. 5b. The bandgap of NbO is found to be 3.02 eV, which is found to decrease upon decorating it with RGO (2.8 eV) Further decrease in the bandgap of NbO/RGO is observed upon doping it with Sr (0.75%) and the observed bandgap of Sr@N/R-0.75% is found to be 2.6 eV which is highly desired in light-driven photocatalytic reactions. Doping of Sr to the NbO/RGO nanocomposite probably created the defects in the structure and shows a decrease in bandgap and could enhance the photocatalytic property due to decreased bandgap and effective separation of photoexcited charge carriers.

Fig. 6 shows the adsorption-desorption isotherms for NbO, NbO/RGO, and Sr@N/R 0.75%. The adsorption-desorption isotherms of all samples are of isothermal type-IV with a hysteresis cycle, which indicates a mesoporous structure according to the IUPAC classification. The BET surface area samples have been determined to be respectively 57.3, 98.7, and 107.4 $m^2 g^{-1}$. NbO particles had the lowest surface area,

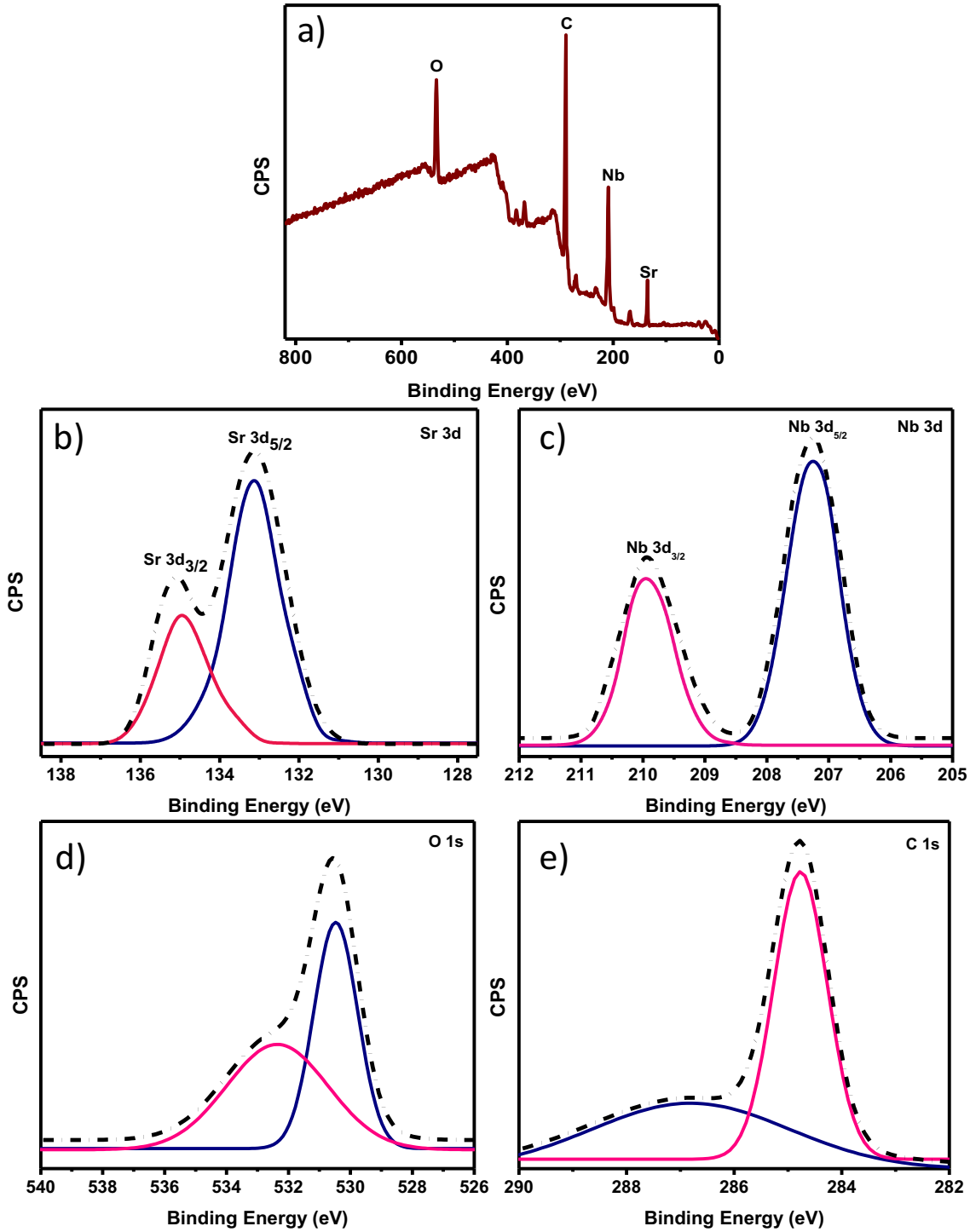

Fig. 4. XPS of Sr@N/R-0.75% nanocomposite a) Survey spectrum b) Sr 3d, c) Nb 3d d) O 1 s and e) C 1 s.

but following the addition of RGO, there is a significant increase in surface area. This may be because the accumulation of NbO particles on the surface may have increased the stacking structure and also decreased agglomeration. Doping of metals enhances the surface area of NbO/RGO due to pore plugging.

3.2. Photocatalytic hydrogen evolution

Hydrogen evolution in presence of UV light has been evaluated under different conditions. The amount of hydrogen evolved (Fig. 7a) is in the order of Sr@N/R-0.75% > Sr@N/R-1% > Sr@N/R-0.5% > Sr@N/R-0.25% > NbO > NbO/RGO > NbO > RGO. The activity of NbO (586 μmol) towards H_2 evolution was found to enhance upon the addition of RGO (986 μmol). Further enhanced catalytic behavior of NbO/RGO is observed upon doping Sr. The effect is found to be linear from 0.25 to 0.75% of Sr doping to N/R nanocomposite and found to decline slightly at 1% Sr. The linear increase in Sr doping from 0.25 to 0.75% could be attributed to availability of easy mobility of electrons, formation of defects and found to decrease after 0.75% Sr doping probably due to the agglomeration of the nanocomposite. The maximum H_2 evolution is

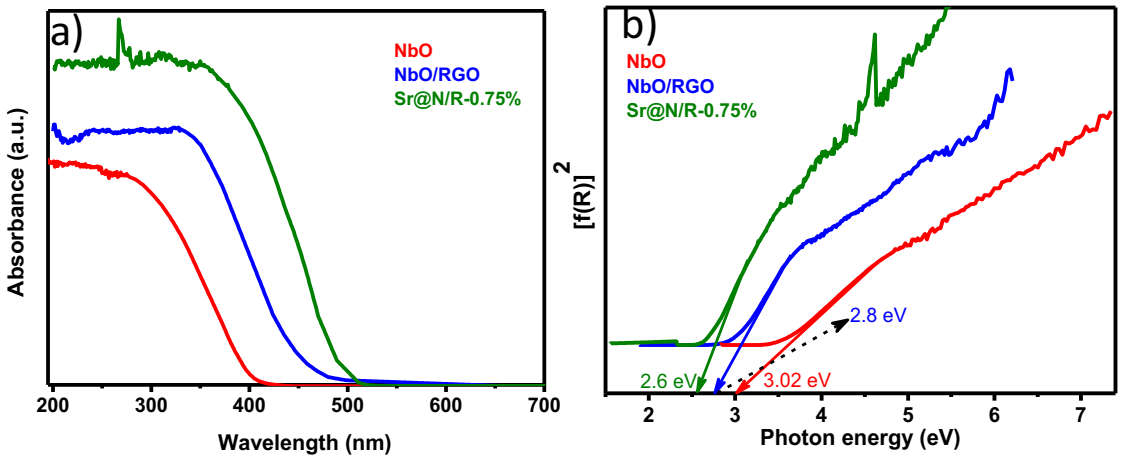

Fig. 5. 5a) UV–Vis spectra of NbO, NbO/RGO and Sr@N/R-0.75% nanocomposite.
5b) Kubelka-Munk curves of NbO, NbO/RGO and Sr@N/R-0.75% nanocomposite.

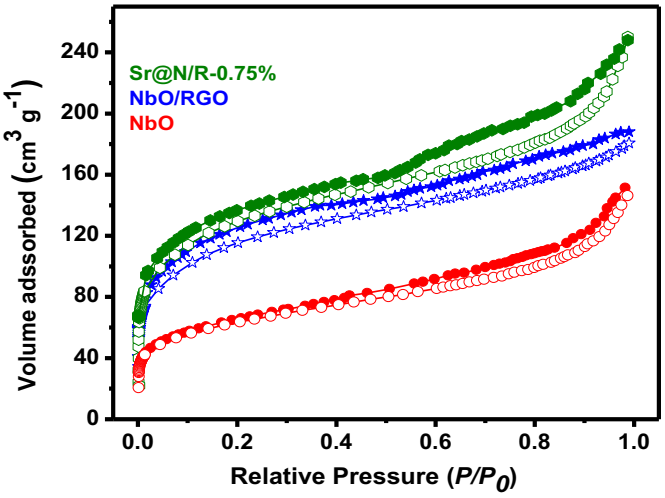

Fig. 6. N_2 adsorption/desorption curves of NbO, NbO/RGO and Sr@N/R-0.75% nanocomposite.

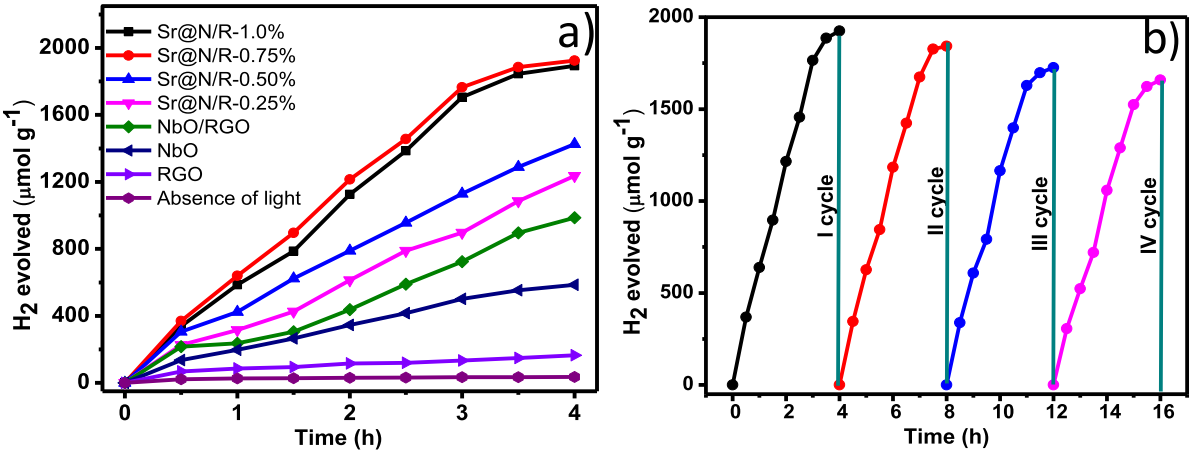

Fig. 7. a) Hydrogen evolution under different conditions.
b) Stability study of Sr@N/R-0.75% nanocomposite towards H_2 evolution.

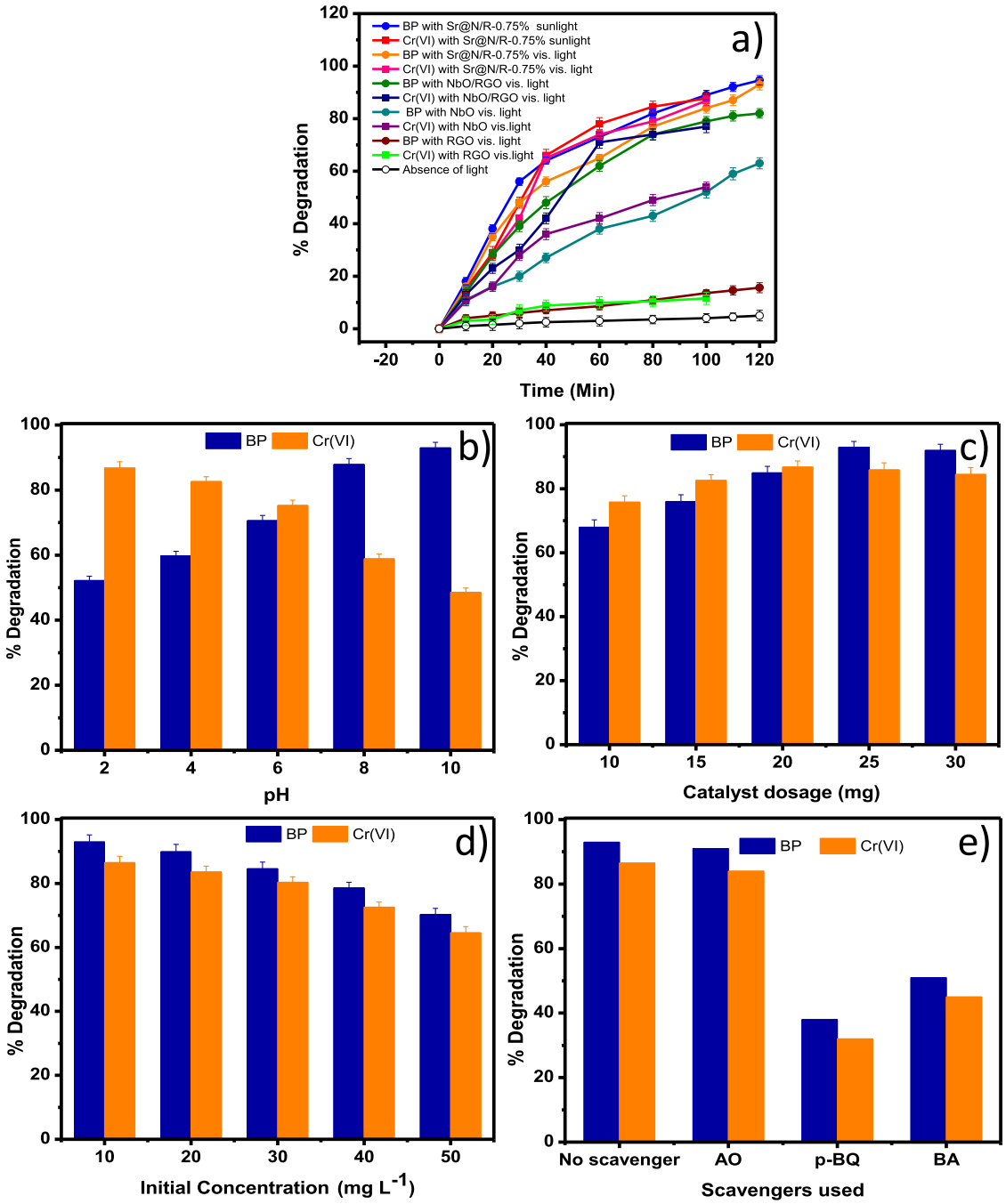

Fig. 8. a) Degradation of BP and Cr(VI) under different conditions.
b) Effect of pH
c) Effect of catalyst dosage
d) Effect of initial concentration
e) Scavenger studies.

observed in Sr@N/R-0.75% and found to be 1925 μmol of H_2 evolution which is almost 2 times higher than NbO/RGO. Sr doping to the nanocomposite shows superior light-driven activity probably attributed to the decreased bandgap, increased defects, and lowered recombination of photoexcited electrons and holes. The stability studies of Sr@N/R-0.75% towards hydrogen evolution (Fig. 7b) show good reusability of the catalyst even after the 4th cycle speaks about good stability.

3.3. Photocalytic degradation studies

Two different sample solutions (benzophenone-3 and Cr(VI)) were evaluated to understand the catalytic property of synthesized materials towards their degradation under different conditions. The degradation of BP and Cr(VI) is almost nil under dark conditions (Fig. 8a). Upon illuminating with visible light in presence of RGO, a slight degradation is observed. NbO was able to degrade 54 and 63% of Cr(VI) and BP in a time of 100 and 120 min, respectively. In presence of NbO/RGO nanocomposite, 77 and 82% of Cr(VI) and BP degradation is observed.

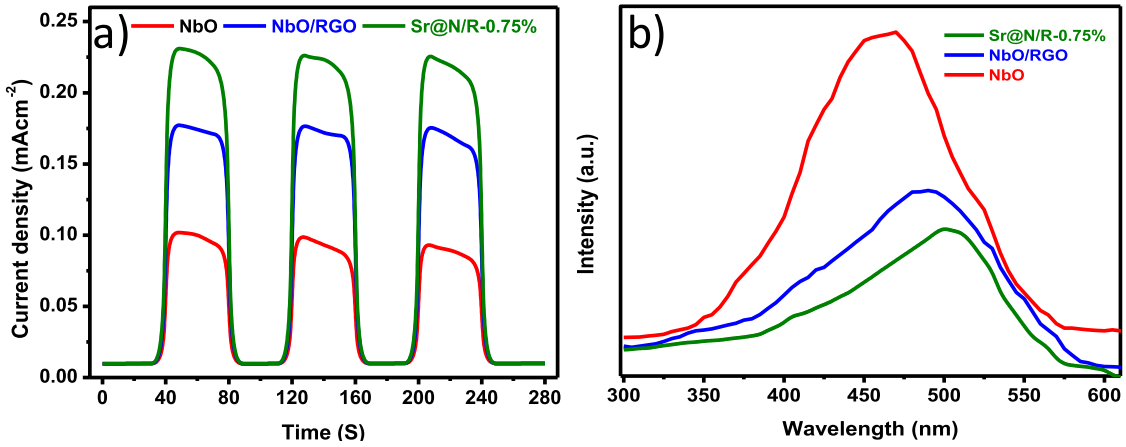

Fig. 9. a) Transient Photocurrent response of NbO, NbO/RGO and Sr@N/R-0.75% nanocomposite.
b) Photoluminescence spectra of NbO, NbO/RGO and Sr@N/R-0.75% nanocomposite.

Sr@NbO/RGO nanocomposite exhibit enhanced activity compared to Sr@NbO/GO nanocomposite as observed in Fig.S4. A further increase in the efficiency of NbO/RGO is observed in Sr@N/R-0.75% and found to degrade 86.8 and 93% of Cr(VI) and BP (The superior efficiency of Sr@N/R-0.75% towards the degradation of both BP and Cr(VI) compared with other % of Sr doping in Sr@N/R nanocomposite as shown in Fig. S5). The ability of Sr@N/R-0.75% was further examined for degradation of BP and Cr(VI) under sunlight. The efficiency of Sr@N/R-0.75% towards the degradation of BP and Cr(VI) under sunlight is high and found to be 94.6 and 87.6%, respectively. The enhanced activity observed under sunlight is probably due to the involvement of both visible and UV radiations. The bandgap engineering of NbO upon decorating with RGO and Sr doping worked well in the photocatalytic activity of NbO. The superior activity in Sr@N/R-0.75% could be attributed to the lowered bandgap, enhanced surface area, and conductivity, and ability to pull out the electrons by Sr from CB without allowing them for recombination.

Though the efficiency of Sr@N/R-0.75% is high under sunlight, optimizations of the different parameters were examined under visible light sources due to variation in the light flux under sunlight. The pH of the reaction medium is one of the key features in photocatalysis. The Fig. 8b indicates the effect of pH on the degradation and detoxification of BP and Cr(VI in presence of Sr@N/R-0.75%. For Cr(VI) the efficiency of Sr@N/R-0.75% was high at pH 2 which is found to decrease upon an increase in the pH value. The proficient degradation of Cr(IV) takes place under acidic conditions only. In contrast, the efficiency of Sr@N/R-0.75% towards the degradation of BP is less under the acidic condition which is found to increase upon raise in the pH and the maximum is observed at pH 10. BP exhibits its molecular structure below its pKa (8.06) and stability is high in acidic condition [24]. At basic pH more hydroxyl ions would be generated which also increases the number of hydroxyl radicals. Due to the higher amount of hydroxyl radicals in the medium, the photocatalytic degradation of BP is highly influenced at pH 10.

The amount of catalyst is one of the important features in photocatalytic degradation studies. The property of a catalyst will be considered as a favor if the amount used is less and the degradation ability is more. The amount of Sr@N/R-0.75% varied from 10 to 30 mg

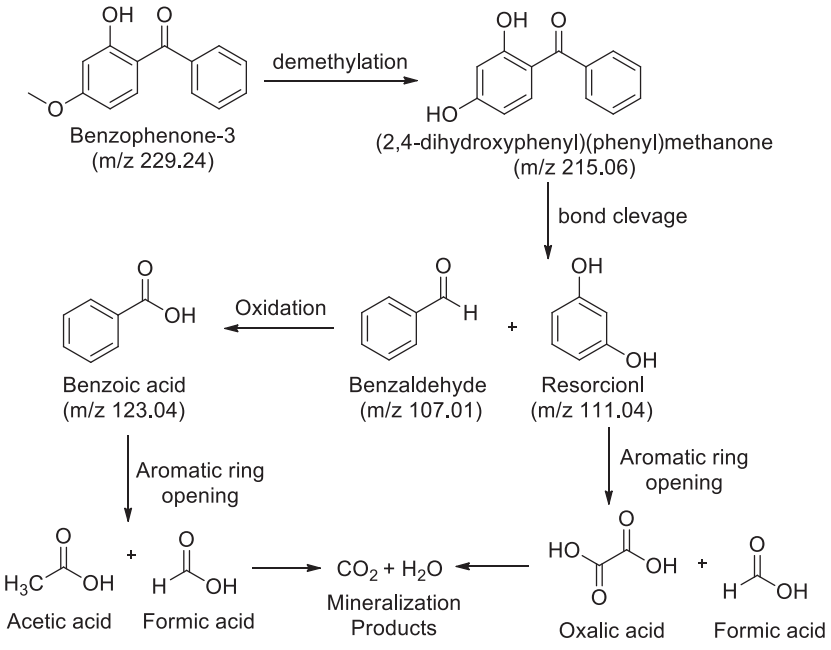

Scheme 2. Degradation pathway of benzophenone-3.

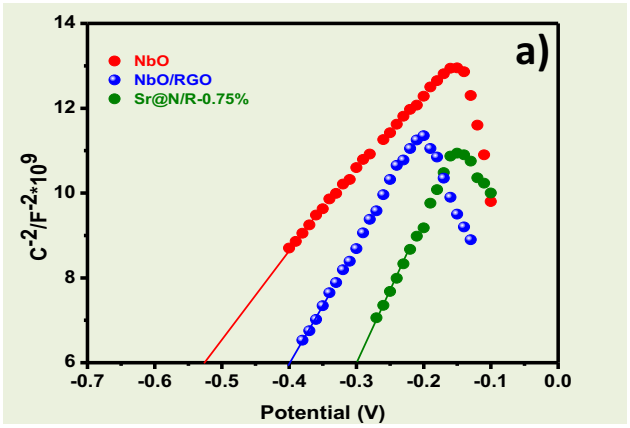

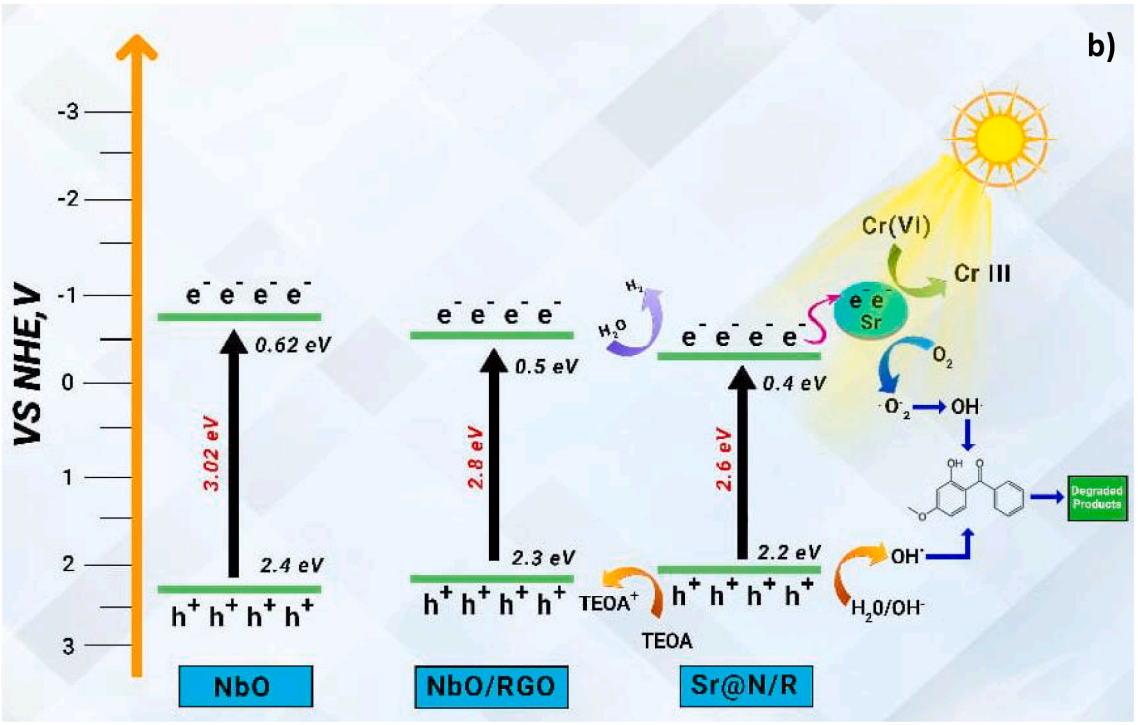

Fig. 10. a) Mott–Schottky plots of NbO, NbO/RGO and Sr@N/R-0.75% nanocomposite at a fixed frequency of 100 Hz.
b) Mechanism of photocatalytic degradation of BP and Cr(VI).

for both samples under study (Fig. 8c). At a lower amount (10 mg) of catalyst, the efficiency was found to be less (68 and 75.8% respectively for Cr(VI) and BP). The maximum detoxification of Cr(VI) was observed when the catalyst used was 20 mg, on the other hand, the maximum degradation was observed for BP in presence of 25 mg of catalyst. Above 20 mg for Cr(VI) and 25 mg for BP, the efficiency was found to decrease slightly due to the development of non-transparent photosystem which will not allow much illumination of light for electron excitation. The effect of the initial concentration of BP and Cr(VI) has been evaluated and the results are depicted in Fig. 8d. The efficiency of photocatalytic degradation was high at lower concentrations under optimized conditions, so 10 mg L^{-1} of BP as well as Cr(VI) has been used for further studies.

Heterogeneous catalysis involved in the degradation of organic and inorganic species mainly depends on the reactive species generated during the reaction. To know the reactive species responsible for the reduction of Cr(VI) and degradation of BP scavenger studies have been evaluated using different scavengers for holes (Ammonium oxalate; AO), superoxide radical (*p*-benzoquinone; p-BQ) and hydroxyl radical (Benzoic acid; BA). The results in Fig. 8e indicate the negligible effect of holes on the photocatalytic activity at the same time the photocatalysis of both samples was greatly affected in the other two cases ($^{\bullet}OH$ and $^{\cdot}O_2^-$). This suggests the involvement of both superoxide and hydroxyl during the degradation of BP and reduction of Cr(VI).

3.4. Photoelectrochemical and photoluminescence studies

Photocatalytic reactions mainly depend on the charge transfer kinetics between NbO, RGO and Sr in Sr@N/R-0.75% nanocomposite. Three intermittent cycles constituting 40 s for each cycle were recorded in switch-on-off mode. The transient current plot of NbO, NbO/RGO and Sr@N/R-0.75% nanocomposite is given in Fig. 9a [25]. Transient photocurrent response of Sr (0.25–1%) doping to NbO/RGO nanoaocomposite is given in Fig. S6. The current response is observed for all the three materials under test, but maximum photocurrent response is observed for Sr@N/R-0.75% which is 2 times higher than NbO. This enhanced current response in Sr@N/R-0.75% could be attributed to the occurrence of defects upon doping Sr and layered structure and

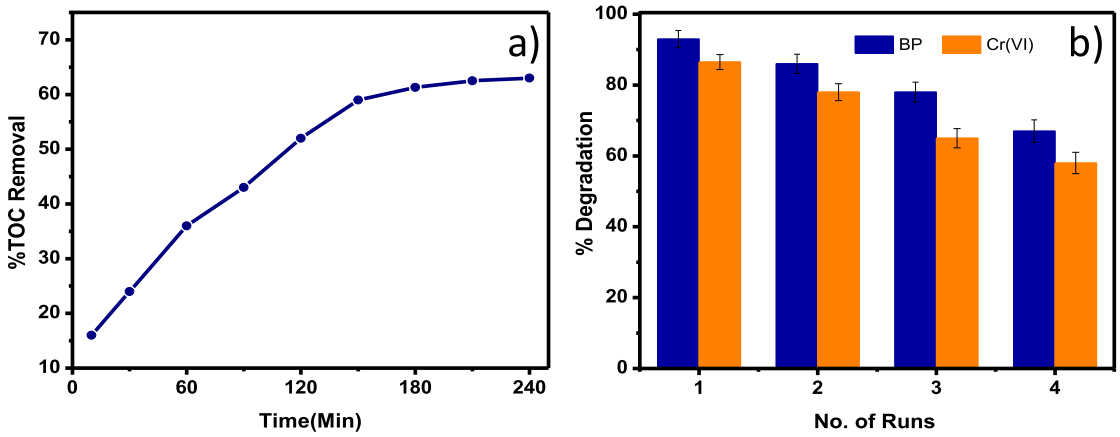

Fig. 11. a) % TOC Removal in swimming pool water sample.
b) Reusability studies of Sr@N/R-0.75% nanocomposite towards degradation of BP and Cr(VI).

enhanced conductivity of RGO accelerate the polarization effect that would enhance the electron distribution during the photocatalytic process. Photoluminescence studies of NbO, NbO/RGO and Sr@N/R-0.75% nanocomposite were conducted and the results are given in Fig. 9b. The intensity of NbO/RGO and Sr@N/R-0.75% nanocomposite has greatly reduced indicating the effective suppression of photoexcited charge carriers. This reduced intensity and a slight blue shift in the peak encompass the enhanced photocatalytic activity of Sr@N/R-0.75% towards the degradation of BP and reduction of Cr(VI).

3.5. Degradation pathway analysis

As a result of photocatalytic degradation, organic carbon and hydrogen are transformed into safe gaseous forms of CO_2 and H_2O, respectively. Under the influence of visible light, benzophenone-3 was photocatalytically degraded in presence of Sr@N/R-0.75% nanocompoiste. The identification of the principal by-products using an LC-MS was done to determine the predominant pollutant breakdown route during the photoredox reaction. Scheme 2 depicts the probable BP degradation pathway as well as demineralization products. The photocatalytic degradation of benzophenone-3 produced several intermediate compounds, some of which were identified, like (2,4-dihydroxyphenyl)(phenyl)methanone (*m/z* 215.06), benzaldehyde (m/z 107.01), resorcinol (m/z 111.04), benzoic acid (m/z 123.06), and oxalic acid (m/z 91.01) as shown in the mass spectra given in Fig. S7. Several studies show that (2,4-dihydroxyphenyl)(phenyl)methanone) is the main product of benzophenone-3 metabolism. Initially, the intermediate (2,4-dihydroxyphenyl)(phenyl)methanone) is generated as a result of demethylation of BP. A likely bond cleavage between the carbonyl group and the aromatic ring bearing the hydroxyl group in their structure owing to the assault of hydroxyl radicals led to the later generation of the by-products benzaldehyde and resorcinol from (2,4-dihydroxyphenyl)(phenyl)methanone. Oxalic acid and formic acid are produced through the aromatic ring opening of the di-hydroxy aromatic molecule resorcinol. In contrast, benzaldehyde that has undergone oxidation produces benzoic acid, which is then converted into aliphatic acids by the breakage of its aromatic ring. Finally, the intermediate carboxylic acids would result in the formation of the demineralization products.

3.6. Mechanism of photocatalysis

The results indicate the occurrence of light-driven reaction between Sr@N/R-0.75% and BP and Cr(VI). By using the insights of degradation pathway, bandgap analysis, photocurrent measurement, and scavenger studies mechanism of photocatalysis has been predicted and is given in Fig. 10. The exact edge potential of the conduction band (CB) was examined using an electrochemical workstation and the obtained Mott-Schottky plot is given in Fig. 10a. The plot indicates n-type nature of all the three materials under study (NbO, NbO/RGO and Sr@N/R-0.75% nanocomposite). The conduction band edge potentials of NbO, NbO/RGO and Sr@N/R-0.75% nanocomposite are found to be 0.62, 0.5 and 0.4 eV. By using this and the obtained bandgap it is easy to locate the edge potential of the valence band (VB) as shown in Fig. 10b. The bandgap of Sr@N/R-0.75% is found to be 2.6 eV, when light radiations are illuminated on the active semiconductor NbO, the electrons in the VB are excited to the CB. During this, the holes present in the CB oxidize the sacrificial agent. The electrons in the CB are utilized by water and evolve hydrogen. In the case of BP and Cr(VI) reduction, the electrons in the CB tend to move to the defects created by Sr as well as RGO sheets [13]. In pristine NbO the photoexcited electrons experience recombination due to poor charge separation and higher bandgap. But in the case of NbO/RGO the charge separation was sufficient enough for photocatalysis. Further enhancement in the photocatalytic efficiency is observed in Sr@N/R-0.75% nanocomposite due to effective inhibition of photoexcited electrons and hole recombination. The synergy, discrete energy levels, decreased bandgap, enhanced surface area and conductivity would help for the swift mobility of electrons that are utilized for the reduction of Cr(VI) to Cr(III) in an acidic medium and presence of light.

$$Cr_2O_7^- + 14H^+ + 6e^- \rightarrow 2Cr^{3+} + 7H_2O$$

During the photoredox reaction of BP, the dissolved oxygen in an aqueous medium utilizes the electrons and reduces to superoxide radical. Superoxide radical in presence of water generates the hydroxyl radical which degrades the BP into carbon dioxide and water as the final eco-friendly products as given in scheme 2.

3.7. Total organic carbon (TOC) removal in swimming pool water and reusability studies

Photocatalytic reactions mainly aim at demineralization of hazardous impurities into environmentally friendly products. Degree of demineralization of BP in presence of light, Sr@N/R-0.75% nanocomposite was subject to analyze the TOC in real sample using analyzer (UV/persulphate TOC removal) in swimming pool water. At first the swimming pool water was collected and prepared a sample solution by adding BP (10 mg L^{-1}). This BP sample solution was subjected to potocatalysis in presence of Sr@N/R-0.75% nanocomposite under optimized conditions. Fig. 11a indicates 63% of TOC removal at 240 min indicates the ability of Sr@N/R-0.75% nanocomposite towards the degradation of BP under light in swimming pool water. Reusability studies of Sr@N/R-0.75% nanocomposite for photocatalytic

Table 1
Comparison of present work with previously reported nanocomposites comprising Nb for hydrogen evolution.

Sl. No.	Material	Condition	Sacrificial agent	H_2 evolution, μm g^{-1}	Ref
1	$KTa_{0.75}Nb_{0.25}O_3$ g-C_3N_4, Pt	300 W Xe, >420 nm	Methanol	86.2	[26]
2	$Ba_5Nb_4O_{15}$ g-C_3N_4	3 W LEDs 420 nm	Oxalic acid	2673	[27]
3	HNb_3O_8 NiS	300 W Xe	Triethanolamine	1519.4	[28]
4	$AgNbO_3$ g-C_3N_4, Pt	300 W Xe, >420 nm	Methanol	88.0	[29]
5	CdS/Nb2O5/ N-doped-graphene	150 W Xe > 400 nm	Na_2S -Na_2SO_3	800	[30]
6	C-doped $KNbO_3$ MoS_2, Pt	300 W Xe	Methanol	1300	[31]
7	**NbO NbO/RGO Sr@N/R-0.75%**	**400 W Xe > 400 nm**	**TEOA**	**586 986 1925**	**Present work**

Table 2
Comparison of degradation of BP with reported methods.

Sl. No.	Material	Optimal condition	% Degradation	Reference
1	TiO_2 coated quartz tube	pH -10 concentration 1 mg L^{-1}, UVC irradiation	98%	[32]
2	TiO_2 (Degussa P-25)	pH -9 concentration 1 mg L^{-1} H_2O_2 concentration 128.06 mg L^{-1}	91.66%	[33]
3	TiO_2 nanowires	pH -4 4 concentration of 20 μM, 180 min UV irradiation (400–360 nm)	90%	[34]
4	PbO/TiO_2–2:1	pH -7 concentration 20 μM	86.6%	[34]
	Sb_2O_3/TiO_2–2:1	pH -9 concentration 20 μM UVC irradiation	80.3%	
5	Fe_2O_3, TiO_2 coated cellulose acetate Cellulose	pH -7, concentration of pollutants: 0.051 μM BP-3 UVC irradiation	90%	[35]
6	**Sr@N/R-0.75%**	**pH -10 concentration 10 mg L^{-1} visible light Sunlight**	** 93% 94.6%**	**Present work**

degradation of BP and reduction of Cr(VI) were examined and the obtained results are given in Fig. 11b. Even after 4 cycles, the Sr@N/R-0.75% nanocomposite showed good stability towards photocatalysis and was able to degrade 67% and 58% of BP and Cr(VI), respectively. decrease in the degradation efficiency probably due to adsorption of the sample on the catalyst surface and thereby blocks the active sites of the catalyst. The results of TOC removal and reusability studies indicate the good stability of the composite for efficient photocatalysis of hazardous organic as well as inorganic species present in water. Overall the efficiency of the synthesized Sr@N/R-0.75% nanocomposite towards hydrogen evolution, degradation of BP and Cr(VI) is high compared to many reported methods as given in Tables 1 and 2 [26–35]. The amount of hydrogen evolved is high, high degree of degradation of BP and Cr(VI) occurred in visible region are the appreciable futures of the present work.

4. Conclusions

An environmentally benign, low-cost, low-energy method has been developed for the synthesis of niobium pentoxide/reduced graphene oxide nanocomposite and studied the effect of different weight % of Sr. It is observed that upon doping Sr to the nanocomposite the material showed enhanced photocatalytic activity due to the formation of defects, discrete energy, enhanced surface area and decreased bandgap. The photocurrent response and photoluminescence results are in good agreement with the obtained results. The hydrogen evolution efficiency of Sr@N/R-0.75% nanocomposite is very good with good stability compared to many reported methods available in the literature. The results of TOC removal in swimming pool water show the practical applicability of the synthesized nanocomposite. UV filter benzophenone degradation in presence of Sr@N/R-0.75% nanocomposite is high and showed efficiency in presence of sunlight which is an add-on advantage of the material for practical applicability. Furthermore, Sr@N/R-0.75% nanocomposite showed its effect on inorganic Cr(VI) reduction in an acidic medium. The results speak about the good stability and reusability of Sr doped NbO/RGO nanocomposite that creates a roadway towards energy and environmental applications.

Credit author statement

K. Yogesh Kumar: Lead investigation and writing.
M.K. Prashanth: Formal analysis and resources and writing.
H. Shanavaz: Conceptualization, lead investigation.
L. Parashuram: Conceptualization, Investigation, Data curation and Writing.
Fahad A. Alharthi: Formal analysis and Resources.
Byong-Hun Jeon: Investigation, formal analysis and resources, review and editing.
M.S. Raghu: Conceptualization, Methodology and writing - review and editing.
Do not have any conflict of interest in publishing article in your Journal.
The authors declare that they have no known competing financial interests or personal relationships that could have appeared to influence the work reported in this paper.

Declaration of Competing Interest

None.

Data availability

Data will be made available on request.

Acknowledgement

The authors are immensely elated and wish to express their indebted gratitude to the Management of NHCE, BNMIT and Jain University for providing lab facilities to carry out this work. Authors are thankful to VGST, Government of Karnataka (GRD-959) for supporting this research. The authors extend their thanks and appreciation to Research Supporting Project (Ref:RSP-2021/160) King Saud University, Riyadh, Saudi Arabia. Byong-Hun Jeon thank Korea Institute of Energy Technology Evaluation and Planning (KETEP) grants funded by the Ministry of Trade, Industry and Energy (MOTIE) of the South Korean Govt. (No.20206410100040) for funding.

Appendix A. Supplementary data

Supplementary data to this article can be found online at https://doi.org/10.1016/j.catcom.2022.106560.

References

[1] S. Cao, J. Yu, g-C_3N_4-based photocatalysts for hydrogen generation, J. Phys. Chem. Lett. 5 (12) (2014) 2101–2107.

[2] H. Furukawa, O.M. Yaghi, Storage of hydrogen, methane, and carbon dioxide in highly porous covalent organic frameworks for clean energy applications, J. Am. Chem. Soc. 131 (2009) 8875–8883.

[3] L. Parashuram, M.K. Prashanth, P. Krishnaiah, C.B. Pradeep Kumar, F.A. Alharti, K. Yogesh Kumar, B.H. Jeon, M.S. Raghu, Nitrogen doped carbon spheres from Tamarindus indica shell decorated with vanadium pentoxide; photoelectrochemical water splitting, photochemical hydrogen evolution & degradation of Bisphenol A, Chemosphere 287 (4) (2021), 132348.

[4] A.S. Alkorbi, K. Yogesh Kumar, M.K. Prashanth, L. Parashuram, A. Abate, F. A. Alharti, B.H. Jeon, M.S. Raghu, Samarium vanadate affixed sulfur self doped g-C3N4 heterojunction; photocatalytic, photoelectrocatalytic hydrogen evolution and dye degradation, Int. J. Hydrog. Energy 47 (26) (2022) 12988–13003.

[5] L. Rizzo, S. Malato, D. Antakyali, V.G. Beretsou, M.B. Đolić, W. Gernjak, E. Heath, I. Ivancev-Tumbas, P. Karaolia, A.R. Lado Ribeiro, G. Mascolo, C.S. McArdell, H. Schaar, A.M.T. Silva, D. Fatta-Kassinos, Consolidated vs new advanced treatment methods for the removal of contaminants of emerging concern from urban wastewater, Sci. Total Environ. 655 (2019) 986–1008.

[6] M. Krause, H. Frederiksen, K. Sundberg, F.S. Jørgensen, L.N. Jensen, P. Nørgaard, C. Jørgensen, P. Ertberg, A. Juul, K.T. Drzewiecki, N.E. Skakkebaek, A. M. Andersson, Presence of benzophenones commonly used as UV filters and absorbers in paired maternal and fetal samples, Environ. Int. 110 (2018) 51–60.

[7] P. Gong, H. Yuan, P. Zhai, Y. Xue, H. Li, W. Dong, G. Mailhot, Investigation on the degradation of benzophenone-3 by UV/H2O2 in aqueous solution, Chem. Eng. J. 277 (2015) 97–103.

[8] M.S. Raghu, L. Parashuram, M.K. Prashanth, K. Yogesh Kumar, C.B. Pradeep Kumar, H. Alrobei, Simple in-situ functionalization of polyaniline with boroncarbonitride as potential multipurpose photocatalyst: generation of hydrogen, organic and inorganic pollutant detoxification, Nano. Str. Nano. Obj. 25 (2021), 100667.

[9] K. Yogesh Kumar, M.K. Prashanth, L. Parashuram, P. Baskaran, A.H. Fahad, B. H. Jeon, Gadolinium sesquisulfide anchored N-doped reduced graphene oxide for sensitive detection and degradation of carbendazim, Chemosphere 296 (2022), 134030.

[10] F. Li, Y. Kang, M. Chen, G. Liu, W. Lv, K. Yao, P. Chen, H. Huang, Photocatalytic degradation and removal mechanism of ibuprofen via monoclinic BiVO4 under simulated solar light, Chemosphere 150 (2016) 139–144.

[11] K. Yogesh Kumar, H. Saini, D. Pandiarajan, M.K. Prashanth, L. Parashuram, M. S. Raghu, Controllable synthesis of TiO_2 chemically bonded graphene for photocatalytic hydrogen evolution and dye degradation, Catal. Today 340 (2020) 170–177.

[12] T.N. Vinuth Raj, P.A. Hoskeri, H.B. Muralidhara, B.P. Prasanna, K. Yogesh Kumar, F.A. Alharthi, M.S. Raghu, Tantalum pentoxide functionalized nitrogen-doped reduced graphene oxide as a competent electrode material for enhanced specific capacitance in a hybrid supercapacitor device, J. Alloys Compd. 861 (2021), 158572.

[13] B. Boruah, R. Gupta, J.M. Modak, G. Madras, Enhanced photocatalysis and bacterial inhibition in Nb2O5 via versatile doping with metals (Sr, Y, Zr, and Ag): a critical assessment, Nanoscale Adv. 1 (2019) 2748.

[14] T.N. Vinuth Raj, Priya A. Hoskeri, H.B. Muralidhara, C.R. Manjunatha, K. Yogesh Kumar, M.S. Raghu, Facile synthesis of perovskite lanthanum aluminate and its green reduced graphene oxide composite for high performance supercapacitors, J. Electro. Anal. Chem. 858 (2020), 113830.

[15] S. Sood, A. Umar, S.K. Mehta, A. Sinha, S.K. Kansal, Efficient photocatalytic degradation of brilliant green using Sr-doped TiO2 nanoparticles, Ceram. Int. 41 (2015) 3533–3540.

[16] M.H. Kabir, A. Bhattacharjee, M. Manjoru Islam, M.S. Rahman, Md.S. Rahman, M. K.R. Khan, Effect of Sr doping on structural, morphological, optical and electrical properties of spray pyrolizedCdO thin films, J. Mater. Sci. Mater. Electron. 32 (2021) 3834–3842.

[17] S. Shanavas, M.A. Haija, D. Pratap Singh, T. Ahamad, S.M. Roopan, Q.V. Le, P. M. Roberto Acevedo, Anbarasan, Development of high efficient Co3O4/Bi2O3/rGO nanocomposite for an effective photocatalytic degradation of pharmaceutical molecules with improved interfacial charge transfer, J. Env. Chem. Eng. 10 (2) (2022), 107243.

[18] S. Shamaila, A.K.L. Sajjad, S. Shaheen, A. Iqbal, S. Noor, G. Sughra, U. Ali, A cost effective and eco-friendly green route for fabrication of efficient graphene nanosheets photocatalyst, J. Environ. Chem. Eng. 5 (6) (2017) 5770–5776.

[19] S. Hamed, A.E. Soleimani, Green synthesis of Ag/Fe_3O_4/RGO nanocomposites by Punica Granatum peel extract: catalytic activity for reduction of organic pollutants, Int. J. Hydrog. Energy 44 (5) (2019) 2711–2730.

[20] T.J.I. Edison, M.G. Sethuraman, Biogenic robust synthesis of silver nanoparticles using Punica granatum peel and its application as a green catalyst for the reduction of an anthropogenic pollutant 4-nitrophenol, Spectrochim. Acta A 104 (2013) 262–264.

[21] M. Çam, Y. Hışıl, Pressurised water extraction of polyphenols from pomegranate peels, Food Chem. 123 (3) (2010) 878–885.

[22] W.S. Hummers, R.E. Offeman, Preparation of graphitic oxide, J. Am. Chem. Soc. 80 (1958) 1339.

[23] B. Pilarek, A.J. Pelczarska, I.S. Zczygie, Characterization of niobium(v) oxide received from different sources, J. Therm. Anal. Calorim. (2017), https://doi.org/10.1007/s10973-017-6300-x.

[24] P. Gago-Ferrero, K. Demeestere, M.S. Diaz-Cruz, D. Barcelo, Ozonation and peroxone oxidation of benzophenone-3 in water: effect of operational parameters and identification of intermediate products, Sci. Total Environ. 443 (2013) 209–217, https://doi.org/10.1016/j.scitotenv.2012.10.006.

[25] J.C. Sin, S.M. Lam, H. Zeng, H. Lin, H. Li, L. Huang, K.O. Tham, A.R. Mohamed, J. W. Lim, Enhanced synchronous photocatalytic 4-chlorophenol degradation and Cr (VI) reduction by novel magnetic separable visible-light-driven Z-scheme CoFe2O4/P-doped BiOBr heterojunction nanocomposites, Environ. Res. 212 (2022), 113394.

[26] Z.Q. Chen, P.F. Chen, P.X. Xing, X. Hu, H.J. Lin, Y. Wu, L.H. Zhao, Y.M. He, Rapid fabrication of KTa0.75Nb0.25/g-C3N4 composite via microwave heating for efficient photocatalytic H_2 eVolution, Fuel 241 (2019) 1–11.

[27] K. Wang, Y. Li, J. Li, G. Zhang, Boosting interfacial charge separation of Ba5Nb4O15/g-C3N4 photocatalysts by 2D/2D nanojunction towards efficient visible-light driven H2 generation, Appl. Catal. B Environ. 263 (2019), 117730.

[28] Y.Z. Xia, S.J. Liang, L. Wu, X.X. Wang, Ultrasmall NiS decorated HNb3O8 nanosheeets as highly efficient photocatalyst for H2 eVolution reaction, Catal. Today 330 (2019) 195–202.

[29] P.F. Chen, P.X. Xing, Z.Q. Chen, X. Hu, H.J. Lin, L.H. Zhao, Y.M. He, In-situ synthesis of AgNbO3/g-C3N4 photocatalyst via microwave heating method for efficiently photocatalytic H2 generation, J. Colloid Interface Sci. 534 (2019) 163–171.

[30] Z. Yue, A. Liu, C. Zhanga, J. Huang, M. Zhu, Y. Du, P. Yang, Noble-metal-free hetero-structural CdS/Nb2O5/N-doped-graphene ternary photocatalytic system as visible-light-driven photocatalyst for hydrogen evolution, Appl. Catal. B Environ. 201 (2017) 202–210.

[31] J.X. Yu, Z.Q. Chen, Q.Q. Chen, Y. Wang, H.J. Lin, X. Hu, L.H. Zhao, Y.M. He, Giant enhancement of photocatalytic H2 production over KNbO3 photocatalyst obtained via carbon doping and MoS2 decoration, Int. J. Hydrog. Energy 43 (2018) 4347–4354.

[32] N. Moradi, M.M. Amin, A.Z. Fatehizadeh, Ghasemi, Degradation of UV-filter Benzophenon-3 in aqueous solution using TiO2 coated on quartz tubes, J. Environ. Health Sci. Eng. 16 (2018) 213–228.

[33] M. Saracino, L. Pretali, M.L. Capobianco, S.S. Emmi, M.L. Navacchia, F. Bezzi, C. Mingazzini, E. Burresi, A. Zanelli, Titania nano-coated quartz wool for the photocatalytic mineralisation of emerging organic contaminants, Water Sci. Technol. 77 (2018) 409–416.

[34] L. Soto-Vázquez, F. Rolón-Delgado, K. Rivera, M.C. Cotto, J. Ducongé, C. Morant, S. Pinilla, F.M. Márquez-Linares, Catalytic use of TiO_2 nanowires in the photodegradation of Benzophenone-4 as an active ingredient in sunscreens, J. Environ. Manag. 247 (2019) 822–828.

[35] H. Zúñiga-Benítez, C. Aristizábal-Ciro, G.A. Peñuela, Heterogeneous photocatalytic degradation of the endocrine-disrupting chemical Benzophenone-3: parameters optimization and by-products identification, J. Environ. Manag. 167 (2016) 246–258.